

NUMERICAL TESTS OF A PHASE FIELD MODEL WITH SECOND ORDER ACCURACY*

GUNDUZ CAGINALP[†], XINFU CHEN[†], AND CHRISTOF ECK[‡]

Abstract. Numerical computations are performed for a recently derived phase field model for the interface between two phases. The rigorous results indicate that solutions to this new phase field model should converge more rapidly than traditional ones to solutions of the corresponding sharp interface (free boundary) formulation for sufficiently small values of the approximation parameter ε representing the thickness of the interfacial region. In particular, the distance between the sharp interface of the limiting model and the zero level set of the phase function in the phase field model is of order ε^2 rather than ε . Numerical computations within a three-dimensional spherically symmetric setting compare the computed solutions of this new model with the known exact solutions for the limiting free boundary problem and confirm the second order accuracy predictions of the theory for sufficiently small ε . The sets of parameters include those of succinonitrile used in dendritic experiments.

Key words. phase field model, matched asymptotic expansion, second order accuracy

AMS subject classifications. 80A22, 80M35

DOI. 10.1137/070680965

1. Introduction. Phase field models are now established as one of the most popular approaches for the computation of various types of dynamical phase transition models and problems with moving interfaces [4, 12, 13, 19, 20, 21, 22, 23, 35].

From the perspective of numerical simulation, these models can be interpreted as approximations of free boundary problems by problems without explicit interface conditions. This simplifies the numerical implementation of the model and, in particular, renders possible the application of standard software packages for partial differential equations (PDEs) to free boundary problems without implementing special front tracking and difficult treatment of topological change techniques. The required resolution for the diffuse interface that arises in the phase field models can be achieved by adaptive mesh refinement, a feature that is typically available in modern software packages.

Although the phase field (diffuse interface) approach can be used within a number of physical applications, many of the key ideas can be understood in terms of the two-phase problem with surface tension and kinetic undercooling. Starting with the free boundary approach for this physical problem, we consider a material in a spatial region $\Omega \subset \mathbb{R}^n$ ($n \geq 1$) that can be in either of two phases (e.g., liquid or solid) separated by an interface, $\Gamma(t)$. Hence the mathematical problem consists of determining both the temperature $T(x, t)$ and the interface $\Gamma(t)$ from the system, in its full dimensional form,

*Received by the editors January 25, 2007; accepted for publication (in revised form) January 28, 2008; published electronically May 28, 2008.

<http://www.siam.org/journals/siap/68-6/68096.html>

[†]Department of Mathematics, University of Pittsburgh, Pittsburgh, PA 15260 (caginalp@pitt.edu, <http://www.pitt.edu/~caginalp>; xinfu@pitt.edu, <http://www.pitt.edu/~xfc>). The second author was supported by National Science Foundation grant DMS-0504691.

[‡]Faculty of Mathematics, University of Bielefeld, Universitätsstr. 25, 33615 Bielefeld, Germany (eck@math.uni-bielefeld.de, <http://www.math.uni-bielefeld.de/~eck>).

$$(1.1) \quad \begin{cases} (\rho c T)_t = \operatorname{div}(K \nabla T) & \text{in } \Omega \setminus \Gamma(t), \\ \rho \ell v_n = \llbracket K \nabla T \cdot \mathbf{n} \rrbracket_+^- & \text{on } \Gamma(t), \\ T = T_E - \frac{\sigma}{[s]_E} \{\kappa + \alpha v_n\} & \text{on } \Gamma(t), \end{cases}$$

with ℓ and c as the latent heat and heat capacity per unit mass, K the diffusivity, ρ the density, T_E the equilibrium freezing temperature, $[s]_E$ (energy/(volume · degree)) the entropy difference per volume, σ (energy/area) the surface tension, and α the strength of kinetic undercooling. The unit normal, sum of principal curvatures, and velocity of the interface are given by \mathbf{n} , κ , and v_n , while $\llbracket \cdot \cdot \rrbracket_+^-$ denotes the difference in the limits from the two sides of the interface.

The history of this problem dates back to 1831 when Lamé and Clapeyron [25] studied the freezing of the ground using (1.1) with $T = T_E$ replacing the third equation in (1.1). Reformulated in 1889, it became known as the classical Stefan problem [34]. It has the appealing mathematical feature that the temperature, $T(x, t)$, determines the phase at each point (x, t) . By definition, $T(x, t) > T_E$ implies that the material is liquid at that point (or, more generally, in the phase with the higher internal energy), while $T(x, t) < T_E$ means that it is solid, and $T(x, t) = T_E$ defines the interface $\Gamma(t)$. Thus, the condition that $T(x, t) = T_E$ at the interface appears to be mathematically convenient. Nevertheless, the mathematical study of classical solutions to the Stefan model posed difficult challenges. Modern analysis (e.g., [26, 31]) converts (1.1) (with $\sigma = 0$) to the single equation $[e(u)]_t = D \Delta u$, where u is a scaled temperature, $e(u)$ is proportional to internal energy, and $D = K/(\rho c)$ is the heat diffusion coefficient. Since phase is assumed to be determined by temperature, one can write $e(u) = u + H(u)$ with H the Heaviside function.

Materials science research (e.g., [17]) in subsequent decades (after Lamé and Clapeyron [25]) showed that the interface temperature need not be at the equilibrium melting temperature, T_E , so that the material can be liquid well below the melting temperature, for example. In terms of mathematical modeling, there is a profound difference between the classical Stefan model ($T = T_E$ on $\Gamma(t)$) and the modern set of equations (1.1), since the temperature in the latter model can no longer retain its dual role of determining both the temperature and the phase. This means that using (1.1) directly necessitates tracking the interface in time, which is difficult but mathematically possible; see [15] for the well-posedness of the problem. Even if this is done, however, equations (1.1) are valid only so long as the interface does not self-intersect.

An alternative approach, known as the phase field or diffuse interface model, is to formulate the problem in terms of two variables, temperature and phase field (see [10] for more discussion). The mathematical problem is then to solve the following parabolic system for $(T_\varepsilon, \phi_\varepsilon)$ in its full dimensional form:

$$(1.2) \quad \begin{cases} (\alpha_\varepsilon \phi_\varepsilon)_t = \Delta \phi_\varepsilon - \varepsilon^{-2} W'(\phi_\varepsilon) + \varepsilon^{-1} [s]_E \sigma^{-1} G'(\phi_\varepsilon) [T_\varepsilon - T_E], \\ (\rho c T_\varepsilon + \frac{1}{2} \rho \ell \phi_\varepsilon)_t = \operatorname{div}(K \nabla T_\varepsilon), \end{cases}$$

where the unknowns $T_\varepsilon(x, t)$ and $\phi_\varepsilon(x, t)$ are, respectively, the temperature and the phase indicator ($\phi_\varepsilon = 1$ for liquid and -1 for solid) and ε is a small positive parameter representing the thickness of the interfacial region. Here W is a potential with double well of equal depth at ± 1 and G is a function relating microscopically how energy is relayed in the thin interfacial region. As discussed in full in [10], in order for the phase field model to approximate accurately the free boundary model (1.1), it is better to require G and α_ε to satisfy certain compatibility conditions; in particular,

the following choice is sufficient:

$$(1.3) \quad W(s) = \frac{1}{2}(1-s^2)^2, \quad G(s) = s - \frac{1}{3}s^3, \quad \alpha_\varepsilon = \alpha + \frac{5}{12} \frac{\varepsilon \rho \ell [s]_{\mathbb{E}}}{(K\sigma)}.$$

The interface in this formulation is now defined as the level set

$$(1.4) \quad \Gamma_\varepsilon(t) := \{x \in \Omega(t) \mid \phi_\varepsilon(x, t) = 0\};$$

thus there is no need to track it explicitly, and the practical problem is simply the computation of a smooth system of parabolic differential equations. A number of works (e.g., Caginalp and Chen [8, 9] and Soner [33]) have proved that solutions of the phase field equations converge to those of the corresponding free boundary problems as $\varepsilon \rightarrow 0$. The parameter ε represents the thickness of the interfacial region, whose true value is on an atomic scale. Computing with this true physical value would make many realistic computations unfeasible. However, it has been shown that the value of ε can be used essentially as a free parameter that can be increased by orders of magnitude without significantly altering the behavior of the interface [12]. Although the phase field approach provides a methodology for understanding the physical interface problems directly and has been used to derive the sharp interface models, one can also view it as a computational approach designed to approximate the limiting sharp interface (free boundary) problem. This is the perspective we adopt in this paper.

The use of phase field computations in realistic physical situations has led to a growing interest in developing and testing different phase field equations that better approximate the limiting free boundary problem. Let $\Gamma(t)$ and $\Gamma_\varepsilon(t)$ denote the interface of the free boundary problem (1.1) and the zero level set of the phase function $\phi_\varepsilon(x, t)$ of the phase field model (1.2), respectively. We are interested in approximating the free boundary problem with the phase field model by the following criteria: there exist positive constants C and ε_0 such that

$$(1.5) \quad \text{distance}(\Gamma(t), \Gamma_\varepsilon(t)) \leq C\varepsilon^k \quad \forall \varepsilon \in (0, \varepsilon_0].$$

Established theoretical results (e.g., [8, 9]) and computations (e.g., [13, 19]) indicate that these estimates are valid for $k = 1$. Recently, in [10] we derived a phase field model that ensures a second order accuracy (namely, $k = 2$ in the bound above) for the approximation of the free boundary. Unlike the automatic [29] second order approximation of motion by mean curvature by the Allen–Cahn equation [2], the second order accuracy here is obtained by special choices of G and α_ε . In particular, by utilizing the choice (1.3), all first order terms automatically cancel out, thus leading to a second order model. Here the coefficient $\frac{5}{12}$ for the first order correction of α_ε is calculated from the special choices of W and G . The derivation and proof use a method that differs from the standard technique of matched asymptotic expansions [1, 6, 9, 11, 16]. In our recent work, the inner expansion is computed with respect to the interface $\Gamma(t)$ of the limit interface and not with respect to the level set $\Gamma_\varepsilon(t)$ of the phase field as in more traditional approaches. A key advantage of this new technique is that it permits tracking of the position of the perturbed interface by a distance function h_ε to the limit interface; see section 2.

There have been other studies attempting to derive phase field models that converge more rapidly to their sharp interface limits by an alternative procedure of finding conditions that eliminate undesired terms of first order, as done, e.g., in [3]. It is not

always obvious, however, which terms should be cancelled in order to obtain robust approximation properties that are an improvement over the original models.

The rigorous theory does not establish the constant C in the estimates (1.5) or the value of the upper bound ε_0 for which the bounds are valid. Consequently, we perform numerical computations on this recently derived phase field equation to determine whether the second order accuracy described by these bounds is valid for typical parameter ranges and computational constraints. In particular, one of the tests utilizes the physical measurables for succinonitrile that is used in many of the dendritic experiments [18, 24].

2. The phase field model. In this section, we state the phase field model (1.2) introduced in [10] in a form that is convenient for computation.

2.1. Nondimensionalization. Using the fully physical dimensional form of equations has its advantage and convenience for practical considerations. Mathematically, however, it is awkward and numerically complicated in realizing the stiffness of the problem. From the viewpoint of scaling invariance, it is desirable to make a change of variables to transfer the fully dimensional version of the free boundary problem (1.1) and the phase field model (1.2) into their nondimensional counterparts.

To convert (1.1), introduce L , the diameter of the sample, and use the standard transformation

$$u := \frac{T - T_E}{\ell/c}, \quad D := \frac{K}{\rho c}, \quad d_0 := \frac{\sigma c}{[s]_E \ell}, \quad a := \alpha D,$$

$$d := \frac{d_0}{L}, \quad \frac{x}{L} =: \tilde{x} \longrightarrow x, \quad \frac{D}{L^2} t =: \tilde{t} \longrightarrow t.$$

The free boundary problem (1.1) then has the following dimensionless form:

$$(2.1) \quad \begin{cases} u_t^\pm = \Delta u^\pm & \text{in } \Omega^\pm(t), \\ u^\pm = -d(\kappa + av) & \text{on } \Gamma(t), \\ v = \llbracket \nabla u \cdot \mathbf{n} \rrbracket_+^- & \text{on } \Gamma(t), \end{cases}$$

where $\Omega^+(t) \cup \Omega^-(t) \cup \Gamma(t) = \Omega$, \mathbf{n} is the unit vector normal to $\Gamma(t)$ pointing toward $\Omega^+(t)$, κ is the sum of the principal curvatures of $\Gamma(t)$ (positive for convex solid), and v is the normal velocity of $\Gamma(t)$ (positive for solidification).

Note that the size of the sample (i.e., Ω) in the new, \bar{x} , units is 1 in (2.1). There are only two physical dimensionless parameters: a and d .

1. The constant a represents the strength of kinetic undercooling; it is a measurable *dimensionless material constant*.
2. While d_0 is a *material constant* that relates the surface tension or size of the nucleation radius, the dimensionless constant

$$d := \frac{d_0}{L}$$

depends on the particular experiment. For example, for a typical $d_0 = 10^{-7}$ cm, if the “sample size” or “macroscopic resolution size” is $L = 10^{-3}$ cm, then $d = 10^{-4}$.

Although d is small and the difference between the Gibbs–Thomson condition $u = -d(\kappa + av)$ and the Stefan condition $u = 0$ on the free boundary may appear insignificant, the respective interface motion is known to be significantly different for the two conditions [28, 30].

3. We use a unit for time that matches the units of space. For example, if $D = 10^{-3} \text{ cm}^2/\text{s}$ and $L = 10^{-3} \text{ cm}$, then $t = 1000$ represents a physical $L^2t/D = 1$ second. In other words, $t = 1$ represents one millisecond.
4. Here $u = 1$ represents the temperature that a liquid at melting temperature attains after absorbing an amount of energy equal to the latent heat. For water, $u = 1$ represents $T = 80^\circ \text{ C} = 353 \text{ Kelvin}$. In this problem there is another parameter, u_∞ , the dimensionless temperature at the far field, that plays a role. When u_∞ is small, quite often it is convenient to use $u/|u_\infty|$ as the dimensionless temperature. For succinonitrile, $\ell/c = 23.13 \text{ Kelvin}$, so $T_\infty = T_E - 0.2313 \text{ Kelvin}$ is equivalent to $u_\infty = -0.01$.

In addition to the dimensionless quantities above, it is useful to scale the extra parameter, ε , representing the thickness of interfacial region (5–100 atomic distances). Introducing dimensionless constants

$$\bar{\varepsilon} := \frac{\varepsilon}{d_0}, \quad \epsilon := \frac{\varepsilon}{L} = \frac{\varepsilon}{d_0} \frac{d_0}{L} = \bar{\varepsilon} d,$$

the phase field model (1.2) has the following dimensionless form:

$$(2.2) \quad \begin{cases} u_t + \frac{1}{2}\phi_t = \Delta u, \\ (a + \frac{5}{12}\bar{\varepsilon})\phi_t = \Delta\phi + \epsilon^{-2}(2\phi + \bar{\varepsilon}u)(1 - \phi^2). \end{cases}$$

The stiffness of the phase field model comes from the largeness of the quantity ϵ^{-2} on the right-hand side of the second equation. Here the important correction term $\frac{5}{12}\bar{\varepsilon}$ is an addition to the traditional phase field model. It eliminates the first order terms in the asymptotic expansion. As mentioned in the introduction, the applicability of the phase field model in numerical computations is due to the fact that one does not need to use the actual (atomic) size of ϵ . One can use ϵ that is much larger—though still small—without altering the solution significantly [12, 13].

2.2. Initial data. To obtain second order approximation, the initial value to the phase field system (2.2) has to be second order consistent with the free boundary problem (2.1). This leads to the following choice of initial data for (2.2) (see [10] for details):

$$(2.3) \quad \begin{cases} \phi(\cdot, 0) = \tanh \frac{h}{\epsilon}, \\ u(\cdot, 0) = \frac{u_0^+}{1 + e^{-2h/\epsilon}} + \frac{u_0^-}{1 + e^{2h/\epsilon}} + \frac{\epsilon}{2} \nabla h \cdot \nabla (u_0^+ - u_0^-) \int_{-\infty}^{h/\epsilon} z \, d \tanh z. \end{cases}$$

Here $h = h(x)$ is the signed distance from x to the initial interface $\Gamma(0)$, and $u_0^\pm = u_0^\pm(x)$ are smooth extensions of the initial temperature for the free boundary problem.

3. Analytic feature of the numerical example. The main purpose of this paper is to check numerically the validity of the assertion that the new phase field model (2.2) approximates the free boundary model (2.1) with second order accuracy, using physical parameters in one case. In particular, the computations can address the issue of the constants C and ε_0 in (1.5), thereby determining whether there is a computational advantage to the new phase field model in practical circumstances. The test example in our earlier paper [10] is one dimensional, so the curvature effect is not present. We would like to find a test case that has the following features:

1. Explicit solutions for the free boundary problem are available.
2. There are curvature effects.
3. There are kinetic undercooling effects.
4. The ratio between the curvature effect and kinetic undercooling effect can be adjusted.

There is an example in a three dimensional radially symmetric situation that models the solidification (growing) process of a solid ball in undercooled liquid [32]. The solution has the properties that (i) the free boundary is located at $|x| = R(t) = 2\gamma\sqrt{t}$, and (ii) the temperature is a combination of three self-similar solutions to the heat equation $u_t = \Delta u$:

$$\begin{aligned}
 u(x, t) &= u_0 := 1, \\
 u(x, t) &= u_1(|x|, t), & u_1(r, t) &:= \frac{\operatorname{erf}(r/\sqrt{4t})}{r}, & \operatorname{erf}(z) &:= \frac{2}{\sqrt{\pi}} \int_0^z e^{-y^2} dy, \\
 u(x, t) &= u_2\left(\frac{|x|}{\sqrt{4t}}\right), & u_2(z) &:= \int_z^\infty \frac{e^{-y^2}}{y^2} dy.
 \end{aligned}$$

The following calculations verify that for each $\gamma > 0$, there is exactly one such solution to (2.1).

1. When the free boundary is given by $|x| = R(t) := 2\gamma\sqrt{t}$, one has

$$\kappa = \frac{2}{R(t)}, \quad v = \frac{dR(t)}{dt} = \frac{\gamma}{\sqrt{t}} = \frac{2\gamma^2}{R(t)}, \quad \frac{av}{\kappa} = a\gamma^2.$$

The Gibbs–Thomson condition requires the temperature at the free boundary to be

$$u\Big|_{\Gamma(t)} = -d(\kappa + av) = -\frac{A}{R(t)}, \quad A := 2d(1 + a\gamma^2).$$

2. In the ball $\{x \mid |x| < R(t)\}$, the material is in the solid phase. The only self-similar solution to the heat equation $u_t = \Delta u$ with boundary value $u(x, t) = -A/r$ at $r = |x| = R(t)$ and vanishing derivative at $r = 0$ is given by

$$(3.1) \quad u^-(x, t) = -\frac{Au_1(|x|, t)}{\operatorname{erf}(\gamma)}.$$

3. Outside the ball $\{x \mid |x| \leq R(t)\}$, the material is in the liquid phase. There is a family, with parameter B , of solutions having boundary value $u(x, t) = -A/r$ at $r = |x| = R(t)$:

$$(3.2) \quad u^+(x, t) = -\frac{Au_1(|x|, t)}{\operatorname{erf}(\gamma)} + B\left(u_2(\gamma) - u_2(|x|/\sqrt{4t})\right).$$

The solution we need corresponds to that satisfying $v = \llbracket u_r \rrbracket_+^-$. Thus, we have

$$\frac{2\gamma^2}{R(t)} = \frac{Bu'_2(\gamma)}{\sqrt{4t}}, \quad \text{i.e.,} \quad B = \frac{2\gamma}{u'_2(\gamma)} = -2\gamma^3 e^{\gamma^2}.$$

In conclusion, for each $\gamma > 0$ we have a solution to (2.1), given by

$$(3.3) \quad \begin{cases} \Gamma(t) &= \{x \mid |x| = R(t) := 2\gamma\sqrt{t}\}, \\ u(x, t) &= -\frac{2d(1+a\gamma^2)\operatorname{erf}(|x|/\sqrt{4t})}{\operatorname{erf}(\gamma)|x|} - \int_{\gamma}^{\max\{\gamma, |x|/\sqrt{4t}\}} \frac{2\gamma^3 e^{\gamma^2-y^2}}{y^2} dy. \end{cases}$$

For such a solution, the ratio of the strength of the kinetic undercooling to the strength of the surface tension is $av/\kappa = a\gamma^2$. Also, there is an important physical quantity,

$$u_{\infty} := u|_{|x|=\infty} = -2\gamma^3 \int_{\gamma}^{\infty} \frac{e^{\gamma^2-y^2}}{y^2} dy.$$

Given $u_{\infty} < 0$, one can show that there is a unique positive γ that satisfies the above relation. Thus, the measure of the degree of undercooling u_{∞} is equivalent to the measure of γ .

4. Numerical simulation. For a solution (3.3) of the free boundary problem (2.1), we solve numerically the corresponding radially symmetric solution to the phase field model (2.2) in the unit ball:

$$\Omega := \{x \in \mathbb{R}^3 \mid |x| < 1\}.$$

The system (2.2) is first discretized with respect to time by a second order scheme. Fix a time mesh size $\delta t > 0$. For every integer $k \geq 0$, denote by $(u_k(\cdot), \phi_k(\cdot))$ the approximation of the solution $(u(\cdot, k\delta t), \phi(\cdot, k\delta t))$ at time $t = k\delta t$. The semi-discretization in time has the form

$$\begin{aligned} \frac{u_{k+1} - u_k}{\delta t} + \frac{\phi_{k+1} - \phi_k}{2\delta t} &= \Delta \frac{u_{k+1} + u_k}{2}, \\ \epsilon^2 a_{\epsilon} \frac{\phi_{k+1} - \phi_k}{\delta t} - \epsilon^2 \Delta \frac{\phi_{k+1} + \phi_k}{2} &= -W'(\phi_k) - \frac{1}{2}W''(\phi_k)[\phi_{k+1} - \phi_k] \\ &\quad + \frac{\bar{\epsilon}(u_k + u_{k+1})}{2} \left\{ G'(\phi_k) + \frac{1}{2}G''(\phi_k)[\phi_{k+1} - \phi_k] \right\}, \end{aligned}$$

where

$$\bar{\epsilon} := \frac{\epsilon}{d_0}, \quad \epsilon := \frac{\epsilon}{L}, \quad a_{\epsilon} := a + \frac{5}{12}\bar{\epsilon}, \quad W(s) = \frac{1}{2}(1-s^2)^2, \quad G(s) = s - \frac{1}{3}s^3.$$

In the radial ($r = |x|$) coordinates, the Laplacian Δ is further discretized by linear finite elements on a uniform mesh of size $\delta r = 1/n$, where n is the total number of spatial mesh points. This scheme leads to a nonlinear system for each time step.

The boundary condition for temperature of the phase field model is taken as the known exact solution to the free boundary problem, whereas the boundary value for ϕ is taken as $\phi|_{|x|=1} = 1$. The solution is calculated for a time interval $[t_0, t_1]$ according to the timing of the solution (3.3) of the free boundary problem. Here $t_0 > 0$ is the initial time, and the terminal time t_1 satisfies $2\gamma\sqrt{t_1} < 1$. The initial condition (at time $t = t_0$) is taken as (2.3), where $h = h(x) = |x| - R(t_0)$, and u_0^- and u_0^+ are as in (3.1) and (3.2).

In what follows, Model 1 refers to the original phase field model where the correction term $\frac{5}{12}\bar{\epsilon}$ in the kinetic coefficient, a_{ϵ} , is not present; i.e., $a_{\epsilon} = a$. Model 2 is that with the correction added: $a_{\epsilon} = a + \frac{5}{12}\bar{\epsilon}$.

Remark. (1) In our actual implementation, the quantity $\frac{\bar{\epsilon}(u_k+u_{k+1})}{2}$ on the right-hand side of the second equation is replaced by $\bar{\epsilon}u_k$. The advantage of such a change is that the nonlinear system for (ϕ_{k+1}, u_{k+1}) is decoupled into two linear systems, one for ϕ_{k+1} and the other for u_{k+1} . Though theoretically the resulting discretization becomes first order in δt , the discretization is still stable, and in the special case when $\bar{\epsilon}$ is small, this change from $\frac{\bar{\epsilon}(u_k+u_{k+1})}{2}$ to $\bar{\epsilon}u_k$ can be regarded as second order.

(2) The initial condition (2.3) is derived only from model 2; namely, it may not apply to Model 1, where $a_\epsilon = a$. Thus, in numerical implementation for Model 1, the last term in (2.3) is not added in the initial value for u . This is a routine practice in traditional numerical simulations for the phase field models. Indeed, starting from any crude initial data, the phase field dynamics automatically produces a needed fine profile after a small initiation time.

Computation 1. We begin by testing the accuracy of the numerical scheme. That is, for fixed ϵ we find the rate of convergence of the numerical scheme with respect to the spatial mesh size $\delta r = 1/n$ and the time mesh size δt . This helps us to determine how fine a mesh is needed in order to compare the difference between the exact solution to (2.1) and the exact solution to (2.2).

As an illustration, we take the following values of the dimensionless quantities:

$$a = 20, \quad d := \frac{d_0}{L} = 0.001, \quad \bar{\epsilon} = \frac{\epsilon}{d_0} = 5, \quad \epsilon = \frac{\epsilon}{L} = 0.005, \quad u_\infty = -0.0046.$$

The corresponding value of γ and the ratio of kinetic undercooling to curvature effect are, respectively,

$$\gamma = \frac{1}{20}, \quad \frac{a v}{\kappa} = a \gamma^2 = \frac{1}{20}.$$

We calculate the solution from time $t_0 = 1.0$ with initial radius of solid $R(t_0) = 0.1$ to time $t_1 = 9.0$ with final radius $R(t_1) = 0.3$. The numerical result is summarized in Table 1. For easy reference, errors to the exact solution of the phase field model (PFM) and differences to the solution of the free boundary problem (FBP) are calculated in their relative sizes. In calculating the relative error of the numerical scheme here, the exact solution is postulated to be the numerical solution with the finest mesh.

With this assumption we examine the previous level of refinement, namely $n = 3200$, $\delta t = 2.5 \times 10^{-5}$, and observe that the errors relative to the PFM are much smaller than those relative to the FBP. This indicates that the mesh refinement is more than adequate to test how accurately each of the two (phase field) models approximates the FBP. In particular (for $n = 3200$, $\delta t = 2.5 \times 10^{-5}$) the relative error of computation for Model 1 is 10^{-5} , while the difference between the computed and the exact values of the free boundary is 40 times larger at 4×10^{-4} . For Model 2 there is a factor of 17. Examining the prior two levels of refinement ($n = 1600$ and $n = 800$) for Model 1, we see that the relative error (computation compared with the PFM) diminishes from 2×10^{-4} ($n = 800$) to 4.7×10^{-5} ($n = 1600$) to 10^{-5} ($n = 3200$), i.e., factors of about 4, while the relative difference between computation and the FBP varies only from 2.2×10^{-4} ($n = 800$) to 3.7×10^{-4} ($n = 1600$) to 4.0×10^{-4} ($n = 3200$). Hence, the difference between the computed Model 1 and exact FBP stabilizes near 4.0×10^{-4} . The situation is similar for Model 2; i.e., the numerical error in computing the PFM is negligible compared to the difference between the Model (either 1 or 2) and the exact FBP. Note also that halving the time step has a very small effect on these errors.

TABLE 1

Computation 1. The rate of convergence of the numerical scheme, shown in relative error to the partial differential equation (rel. error to PFM). Spatial and time mesh sizes are $\delta r = 1/n$ and δt . Also shown is the relative difference with respect to the solution to the free boundary problem (rel. diff. to FBP). Here $\epsilon = 0.005$.

n ($1/\delta r$)	δt	Model 1			Model 2		
		Position	Rel. error to PFM	Rel. diff. to FBP	Position	Rel. error to PFM	Rel. diff. to FBP
200	4.0 e-4	0.284124	5.3 e-2	5.3 e-2	0.283753	5.4 e-2	5.4 e-2
200	2.0 e-4	0.284529	5.2 e-2	5.2 e-2	0.283945	5.3 e-2	5.4 e-2
200	1.0 e-4	0.284865	5.1 e-2	5.0 e-2	0.294068	5.3 e-2	5.3 e-3
400	4.0 e-4	0.299819	1.0 e-3	6.0 e-4	0.299643	1.0 e-3	1.2 e-3
400	2.0 e-4	0.299853	0.9 e-3	4.9 e-4	0.299676	0.9 e-3	1.1 e-3
400	1.0 e-4	0.299870	0.8 e-3	4.3 e-4	0.299693	0.9 e-3	1.0 e-3
800	2.0 e-4	0.300059	2.1 e-4	2.0 e-4	0.299884	2.3 e-4	3.9 e-4
800	1.0 e-4	0.300063	2.0 e-4	2.1 e-4	0.299889	2.1 e-4	3.7 e-4
800	5.0 e-5	0.300065	1.9 e-4	2.2 e-4	0.299891	2.0 e-4	3.6 e-4
1600	1.0 e-4	0.300110	4.7 e-5	3.7 e-4	0.299937	5.0 e-5	2.1 e-4
1600	5.0 e-5	0.300110	4.7 e-5	3.7 e-4	0.299938	4.7 e-5	2.1 e-4
1600	2.5 e-5	0.300110	4.7 e-5	3.7 e-4	0.299938	4.7 e-5	2.1 e-4
3200	1.0 e-4	0.300121	1.0 e-5	4.0 e-4	0.299949	1.0 e-5	1.7 e-4
3200	5.0 e-5	0.300121	1.0 e-5	4.0 e-4	0.299949	1.0 e-5	1.7 e-4
3200	2.5 e-5	0.300121	1.0 e-5	4.0 e-4	0.299949	1.0 e-5	1.7 e-4
6400	1.0 e-4	0.300124		4.1 e-4	0.299952		1.6 e-4
6400	5.0 e-5	0.300124		4.1 e-4	0.299952		1.6 e-4
6400	2.5 e-5	0.300124		4.1 e-4	0.299952		1.6 e-4

TABLE 2

Computation of interface position at terminal time from the phase field models, in comparison with 0.300000 from the free boundary model.

ϵ	Model 1		Model 2	
	$R_\epsilon(t_1)$	$ 1 - R_\epsilon/R $	$R_\epsilon(t_1)$	$ 1 - R_\epsilon/R $
0.0400	0.29814	6.2 e-3	0.29685	1.0 e-2
0.0200	0.29991	3.1 e-4	0.29924	2.5 e-3
0.0100	0.30015	5.0 e-4	0.29981	6.4 e-4
0.0050	0.30012	4.0 e-4	0.29995	1.7 e-4
0.0025	0.30007	2.4 e-4	0.29999	4.4 e-5
0	0.30000	0	0.30000	0

Thus the computations summarized in Table 1 provide a guide to the error in the numerical computations of the PDEs in terms of the mesh sizes for n and δt . With these numerical errors under control, we can pursue our central goal of distinguishing the differences between the models and the free boundary problems. In what follows we will vary ϵ and examine the behavior of these differences as a function of ϵ . In particular we would like to determine if the difference between Model 2 and the free boundary problem is indeed proportional to ϵ^2 , particularly when we use material parameters that are drawn from experiments of dendrites (see Computation 4 below).

In the following examples, the numerical effects are controlled so that the difference shown can be regarded as that between the solutions to the phase field model (2.2) and to the free boundary model (2.1).

Computation 2. Using a sufficiently fine mesh that eliminates significant numerical error (as discussed above), we perform a set of calculations with the material parameters above. These computations involve a spectrum of values of ϵ , as shown in Table 2, and will be compared with the hypothesized relation

$$(4.1) \quad \left| 1 - \frac{R_\epsilon}{R} \right| \sim C\epsilon^2$$

that has been proved [10] using Model 2 for sufficiently small ϵ . In this first set of computations we explore the large ϵ part of this spectrum. For each model we compute $\log |1 - R_\epsilon/R|$ and plot it against $\log \epsilon$, so that a slope of 2 indicates agreement with (4.1), while a slope of 1 suggests an $O(\epsilon)$ error that is the expected result for Model 1. The results for Model 2 are

$$\log |1 - R_\epsilon/R| = 0.554 + 1.8556 \log(\epsilon)$$

Predictor	Coef	Std Error of Coef
Constant	0.554	0.112
Log(ϵ)	1.8556	0.054

with R-Sq = 99.7% and the F -value for the analysis of variance at 1181. The R-Sq value obtained is a statistical measure (not to be confused with the position R that we have above) that indicates that essentially all of the variation in the data points is explained by the linear model above. The F -value is a measure of the squares of differences between the linear model and the mean relative to the linear model and the data points. For four, five or six data points the F -value needed for 95% statistical confidence is 12, 10, and 9, respectively. A complete discussion of these measures can be found in a basic statistical text such as [27]. The coefficient of $\log(\epsilon)$ is $0.8556/0.054 = 15.84$ or almost 16 standard deviations away from the coefficient value of 1. This yields a p -value that is essentially zero; i.e., there is essentially zero probability that the slope differs from 1 due to randomness. In other words, the null hypothesis that the relative difference between Model 2 and the free boundary problem corresponds to an exponent of 1 must be rejected overwhelmingly (16 standard deviations). The values for Model 2 are plotted using the large dots.

A similar analysis for Model 1 (plotted with small dots) shows that the relative error displays a less regular pattern, yielding a coefficient of 0.832 (i.e., slightly less than a linear relationship), but with a p -value of only 0.154 and an F -value of only 3.61:

$$\log |1 - R_\epsilon/R| = -1.5276 + 0.832 \log(\epsilon).$$

In practical terms, there is a significant improvement from Model 1 to Model 2 that is evident particularly for smaller values of ϵ . For the smallest value tested in these computations, namely, $\epsilon = 0.0025$, one has a ratio of $240/44 = 5.4545$ in the relative differences (between the two models) to the exact free boundary problem. The consistency of the results for Model 2 and the coefficient computed above suggest that the difference between the models grows as ϵ is made smaller.

Computation 3. We solve numerically the phase field model (2.2) with the following parameter values:

$$a = 20, \quad d := \frac{d_0}{L} = 0.001, \quad u_\infty = -0.011, \quad \gamma = 0.08, \quad \frac{aV}{\kappa} = a\gamma^2 = 12.8\%.$$

The parameter ϵ is taken in the following range:

$$\epsilon = \frac{\bar{\epsilon}}{L} \in [0.0025, 0.04], \quad \bar{\epsilon} = \frac{\bar{\epsilon}}{d_0} \in [2.5, 40].$$

The time window is $[0.390625, 3.515625]$ during which the interface moves from $R(t_0) = 0.1$ to $R(t_1) = 0.3$. The numerical results are reported in Table 3 and Figure 1(b).

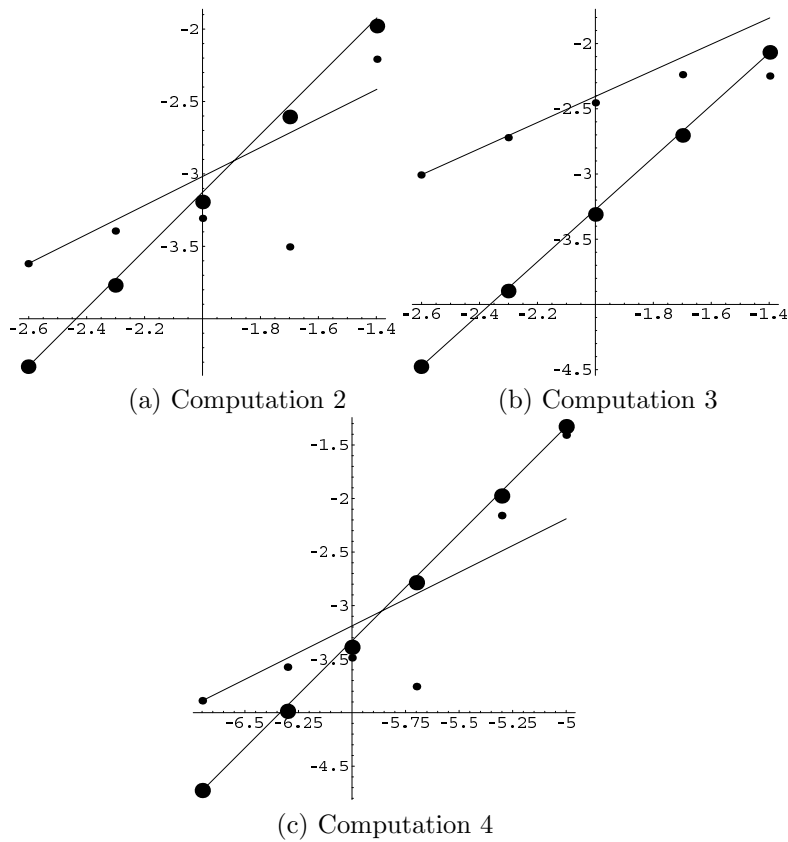


FIG. 1. Horizontal axis is $\log_{10}(\epsilon)$ in (a) and (b) and $\log_{10}(\epsilon/cm)$ in (c). The vertical axis is $\log_{10}|1 - R_\epsilon/R|$. Small dots correspond to Model 1 and large dots to Model 2. Straight lines represent the hypothetical formula $|1 - R_\epsilon/R| = C\epsilon^k$ with $k = 1$ for line with slope 1 and $k = 2$ for line with slope 2.

TABLE 3
For Computation 3.

ϵ	Model 1		Model 2	
	$R_\epsilon(t_1)$	$ 1 - R_\epsilon/R $	$R_\epsilon(t_1)$	$ 1 - R_\epsilon/R $
0.0400	0.30169	5.6 e-3	0.29743	8.6 e-3
0.0200	0.30173	5.8 e-3	0.29941	2.0 e-3
0.0100	0.30105	3.5 e-3	0.29985	4.9 e-4
0.0050	0.30057	1.9 e-3	0.29996	1.3 e-4
0.0025	0.30030	9.9 e-4	0.29999	3.1 e-5
0	0.30000	0	0.30000	0

Performing a least squares analysis as in the previous example for Model 2, we have the result

$$\log|1 - R_\epsilon/R| = 0.741 + 2.01753 \log(\epsilon)$$

Predictor	Coef	Std Error of Coef
Constant	0.74126	0.03563
Log(ϵ)	2.01753	0.07058

with $R\text{-Sq} = 100\%$ and an F -value of 13402. Hence, for these parameters there is overwhelming evidence confirming the hypothetical exponent of 2. The coefficient calculated above differs from 1 by $1.0175/0.07058 = 14.42$ standard deviations.

By comparison the data for Model 1 leads to the result

$$\log |1 - R_\epsilon/R| = -1.21 + 0.661 \log(\epsilon)$$

Predictor	Coef	Std Error of Coef
Constant	-1.21	0.2306
Log(ϵ)	0.661	0.1128

so that the relative difference between Model 1 and the exact free boundary solution behaves as $\epsilon^{0.661}$. A similar regression without the largest value of ϵ leads to $\epsilon^{0.85}$ power behavior.

Thus, one can conclude from this range of computations that Model 2 is within $O(\epsilon^2)$, while Model 1 is even slightly worse than $O(\epsilon)$ in these computations. Note that theorems establishing that Model 1 is $O(\epsilon)$ are also of the form “there exists $\epsilon_0 > 0$ such that for $\epsilon < \epsilon_0$ one has ...” Hence, the data in this range of parameters shows a significant practical improvement by using Model 2 in place of Model 1 that is analogous to the rigorous result.

Computation 4. Finally we provide an example using material data from succinonitrile. We take

$$D = 1.134 \times 10^{-3} \text{cm}^2/\text{s}, \quad d_0 = 2.821 \times 10^{-7} \text{cm}, \quad \frac{\ell}{c} = 23.13 \text{ Kelvin},$$

$$\alpha = 10^4 \text{s/cm}^2.$$

Here D , d_0 , and ℓ/c are from [24]. Note that there are no direct measurements on α and we choose α as in [4].

We focus on the part of the sample of size $L = 10^{-4}$ cm with undercooling $T_E - T_\infty = 0.2521$ Kelvin in a solidification process during which the solid ball grows from radius $R_0 = 10^{-5}$ cm to $R_1 = 4 \times 10^{-5}$ cm.

These dimensional numbers translate to the following dimensionless quantities:

$$a = \alpha D = 11.34, \quad d := \frac{d_0}{L} = 0.002821, \quad u_\infty = -\frac{0.2521}{23.13} = -0.0109,$$

$$\gamma = 0.079, \quad \frac{a v}{\kappa} = a \gamma^2 = 7.2\%, \quad t_0 = \left(\frac{R_0}{2\gamma L}\right)^2 = 0.40, \quad t_1 = \left(\frac{R_1}{2\gamma L}\right)^2 = 6.40.$$

The amount of real time for such a solidification process takes $\frac{(t_1 - t_0)L^2}{D} = 5.2 \times 10^{-5}$ seconds.

To treat such a scenario within the capacity of computer power, we take ϵ in the range 10^{-5} cm to 2×10^{-7} cm. As we said earlier, the true size of ϵ is much smaller, but the interfacial motion is not very sensitive to the size of ϵ provided it is not very large. In dimensionless quantities, this translates to

$$\epsilon = \frac{\epsilon}{L} \in [0.002, 0.1], \quad \bar{\epsilon} = \frac{\epsilon}{d_0} \in [1, 35], \quad \bar{\epsilon} |u_\infty| \in [0.01, 0.35].$$

In Table 4 we list the relative differences between the solution of the phase field model and that of the free boundary problem, with ϵ given in cm.

TABLE 4

For Computation 4, the relative difference between solutions of the free boundary model and solutions of the phase field models 1 and 2.

ϵ (cm)	Model 1		Model 2	
	Position (cm)	$ 1 - R_\epsilon/R $	Position (cm)	$ 1 - R_\epsilon/R $
1 e-5	3.8435 e-5	3.9 e-2	3.8122 e-5	4.7 e-2
5 e-6	3.9723 e-5	6.9 e-3	3.9577 e-5	1.1 e-2
2 e-6	3.9993 e-5	1.8 e-4	3.9935 e-5	1.6 e-3
1 e-6	4.0013 e-5	3.3 e-4	3.9984 e-5	4.1 e-4
5 e-7	4.0011 e-5	2.7 e-4	3.9996 e-5	1.0 e-4
2 e-7	4.0005 e-5	1.3 e-4	3.9999 e-5	1.9 e-5
0	4.0000 e-5	0	4.0000 e-5	0

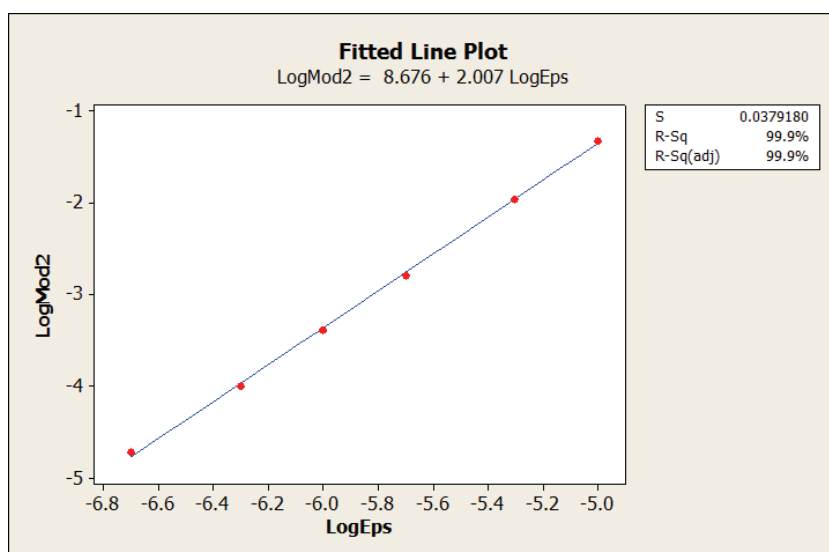


FIG. 2. Computation 4, Model 2.

Using the above procedure on Model 2, we obtain from the least squares analysis the result

$$\log |1 - R_\epsilon/R| = 8.6759 + 2.007 \log(\epsilon)$$

Predictor	Coef	Std Error of Coef
Constant	8.6759	0.1575
Log(ϵ)	2.007	0.02687

Hence, the exponent 2.007 differs from 1 by $1.007/0.02687 = 37.48$ standard deviations, establishing overwhelming evidence that the relative difference between Model 2 and the exact free boundary solution is better than linear in terms of ϵ . One also has that $R\text{-Sq} = 99.9\%$ and $F = 5580$ in the analysis of variance. As shown in Figure 2 the data points are indistinguishable from the straight line with slope 2.007. For this key set of physical parameters, the standard error of 0.02687 shows that the exponent is 2.007 ± 0.02687 so that the computational results are in agreement with the theoretical exponent of 2 in (4.1).

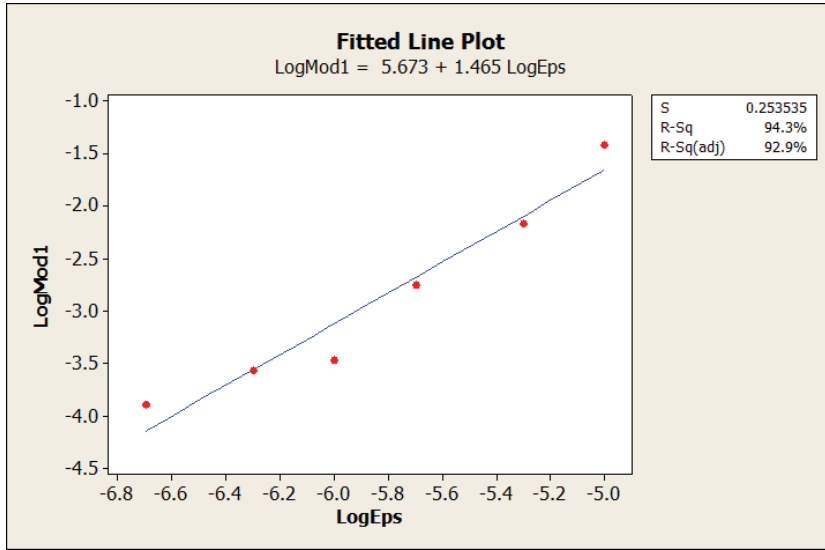


FIG. 3. Computation 4, Model 1.

The same analysis for Model 1 leads to the linear regression

$$\log |1 - R_\epsilon/R| = 5.673 + 1.465 \log(\epsilon)$$

Predictor	Coef	Std Error of Coef
Constant	5.673	1.053
Log(ϵ)	1.465	0.1796

The exponent of 1.47 ± 0.18 appears to be better than the theoretical expectation of 1. Note that the standard error of 0.18 is much larger than the corresponding 0.026 for Model 2 computed above. In Figure 3 one can observe that the slope appears to diminish for smaller ϵ . In particular, for the four smallest values of ϵ , one has the result

$$\log |1 - R_\epsilon/R| = 3.08 + 1.05 \log(\epsilon)$$

Predictor	Coef	Std Error of Coef
Constant	3.08	1.793
Log(ϵ)	1.05	0.2899

Examining the practical differences between the exact solution and those rendered by Models 1 and 2 for the smallest ϵ in Table 4, one observes that the ratio of the error in Model 1 to the error in Model 2 is given by

$$\frac{1.3 \times 10^{-4}}{1.9 \times 10^{-5}} = 6.8421$$

so that a factor of almost seven is attained using Model 1. Note also that the improvement accuracy due to refining ϵ from 5×10^{-7} to 2×10^{-7} is $2.7/1.3 = 2.08$ for Model 1 but $10^{-4}/(1.9 \times 10^{-5}) = 5.2632$ for Model 2. Thus, one would expect that a calculation with $\epsilon = 0.8 \times 10^{-7}$ would lead to a factor of

$$6.8421 \times \frac{5.2632}{2.08} = 17.313.$$

In other words, our analysis shows that for computing capacity that is capable of resolving the phase field model with $\varepsilon = 0.8 \times 10^{-7}$ the error (in approximating the free boundary) in Model 2 would be only $(17.313)^{-1} = 0.05776$, or less than 6% of the error of Model 1. Similarly, for $\varepsilon = 0.32 \times 10^{-7}$ the corresponding ratio would be

$$6.8421 \times \left(\frac{5.2632}{2.08} \right)^2 = 43.809,$$

leading to about 2% of the error.

The rigorous proof of second order convergence [10] is valid for $\varepsilon < \varepsilon_0$ for some positive ε_0 . In any proof of this type one has no assurance that the ε_0 will be large enough to be of any practical significance. In the computations discussed above, particularly the last one in which we utilized material parameters of experiments, it is evident that one obtains this second order convergence using values of ε that are feasible with current computing capacity. Furthermore, there is the issue of the constant in (4.1). Although the constant in (4.1) is larger for Model 2 than for the corresponding expression for Model 1, the factor of ε^2 is small enough to render a much more accurate interface location (relative to the free boundary problem) as discussed above.

Hence, for computations using ε that is about half of the value we have used, one may conclude that our new phase field model (i.e., Model 2) can reduce the error in approximating a free boundary by a factor of 50.

5. Conclusion. We have presented numerical results for a classical phase field model and a new phase field model, demonstrating their asymptotic agreement with a free boundary (sharp interface) model using the Gibbs–Thomson condition and dynamical undercooling at the liquid–solid interface. For both phase field models, the interface, defined as the zero level set of the phase function, is compared with the free boundary of the sharp interface model which is the asymptotic limit of the phase field models. The results confirm the theoretical prediction that the distance between interface and free boundary is of order ε for the classical phase field model and of order ε^2 for the new model. Indeed, these asymptotic behaviors are seen more clearly in the new model than in the classical model. A well-behaved second order accuracy asymptotic behavior of the new model starts from a small ε which is much larger than that of the classical model, which is first order. While the classical model shows considerable deviations from its first order asymptotic behavior of approximating the free boundary model for ε that is not very small, the new model already demonstrates its second order approximation behavior. When ε is small, the new model always leads to a substantially better approximation than the classical one.

The theoretical assertion that the new phase field model is a second order accurate approximation of the free boundary model is derived in [10] from formal expansions in which $1/d := L/d_0$ is regarded as an order one constant and solutions are expanded in $\varepsilon := \varepsilon/L$ power series. Here we omit the details of the formal asymptotic expansions and their rigorous verifications; we refer interested readers to the original formal expansions of Caginalp [5, 7] and rigorous verifications of Caginalp and Chen [9]. In reality it is true that $\varepsilon = \varepsilon/L$ is smaller than $d = d_0/L$, but in numerical simulations such as those demonstrated in this paper, ε is taken as large as d_0 ; i.e., d is as small as ε .

In such a scenario, one can indeed assume that $\bar{\varepsilon} := \varepsilon/d_0 = \varepsilon/d$ is a fixed positive constant, expand the solution in ε or d power series, and demonstrate the following:

1. The leading (zeroth) order expansions of both the new and the classical phase

field models correspond to solutions of the classical Stefan problem, e.g., the solution (3.3) with $d = 0$.

2. The first order expansion of the solution of the new phase field model corresponds to a solution of the free boundary problem (2.1), e.g., the solution (3.3) with $0 < d \ll 1$.
3. The zero level set Γ_ϵ of the phase indicator function ϕ of the new phase field model is $O(\epsilon) = O(\bar{\epsilon}d)$ distance away from the free boundary of the classical Stefan model and is $O(\epsilon^2) = O(\bar{\epsilon}^2d^2)$ distance away from that of the free boundary problem (2.1) (assuming that both free boundary problems admit smooth solutions).
4. On the other hand, the zero level set of the phase function of the classical phase field model is $O(\epsilon) = O(\bar{\epsilon}d)$ distance away from the free boundaries of both the Stefan problem and (2.1).

For the numerics of our current paper, which involve the mathematical limit of ϵ approaching zero, the computations are very close to the exact solutions even if ϵ/d_0 is not small. When $\bar{\epsilon} := \epsilon/d_0$ is large in numerical simulation, the addition of $5\bar{\epsilon}/12$ to the kinetic undercooling coefficient from a to $a_\epsilon = a + 5\bar{\epsilon}/12$ can become significant.

To use the new phase field model (2.2) to approximate (2.1), one needs a resolution of order $o(d)$ at the interface. Since theoretical predication and numerical validation of this paper indicate that the error of this approximation at interface is $O(\epsilon^2)$, what we need is $\epsilon^2 = \bar{\epsilon}^2d^2 = o(d)$, that is,

$$0 < \epsilon \ll \sqrt{Ld_0}.$$

For example, in a dendritic growth experiment [22] with $d_0 = 8 \times 10^{-7}$ cm and $L = 0.8$ cm, the above criterion means that in numerical simulations using the new phase field model (2.2) to capture the Gibbs–Thomson condition, the parameter ϵ used should be smaller than $\sqrt{Ld_0} = 8 \times 10^{-4}$ cm, i.e., $\epsilon = \epsilon/L < 0.001$. This amounts to thousands of grid points in each space dimension and millions of time steps for simulations of real experiments. Hence for values such as $\epsilon = 0.001$, yielding $\bar{\epsilon} = \epsilon/d_0 = 1000$, there is a huge computational advantage in using the new phase field model with $a_\epsilon = a + 5\bar{\epsilon}/12$ replacing a of the traditional phase field model.

REFERENCES

- [1] A. D. ALIKAKOS, P. W. BATES, AND X. CHEN, *Convergence of the Cahn-Hilliard equation to the Hele-Shaw model*, Arch. Rational Mech. Anal., 128 (1994), pp. 165–205.
- [2] S. ALLEN AND J. CAHN, *A microscopic theory for antiphase boundary motion and its application to antiphase domain coarsening*, Acta Metall., 27 (1979), pp. 1085–1095.
- [3] R. F. ALMGREN, *Second-order phase field asymptotics for unequal conductivities*, SIAM J. Appl. Math., 59 (1999), pp. 2086–2107.
- [4] Y. B. ALTUNDAS AND G. CAGINALP, *Computations of dendrites in 3-D and comparison with microgravity experiments*, J. Stat. Phys., 110 (2003), pp. 1055–1067.
- [5] G. CAGINALP, *An analysis of a phase field model of a free boundary*, Arch. Rational Mech. Anal., 92 (1986), pp. 887–896.
- [6] G. CAGINALP, *The role of microscopic anisotropy in the macroscopic behavior of a phase boundary*, Ann. Physics, 172 (1986), pp. 136–155.
- [7] G. CAGINALP, *Limiting Behavior of a Free Boundary in the Phase Field Model*, CMU report 82-5, Carnegie Mellon University, Pittsburgh, PA, 1982.
- [8] G. CAGINALP AND X. CHEN, *Phase field equations in the singular limit of sharp interface problems*, in On the Evolution of Phase Boundaries, IMA Vol. Math. Appl. 43, M. Gurtin, ed., Springer, New York, 1992, pp. 1–27.
- [9] G. CAGINALP AND X. CHEN, *Convergence of the phase field model to its sharp interface limits*, European J. Appl. Math., 9 (1998), pp. 417–445.

- [10] G. CAGINALP, X. CHEN, AND C. ECK, *A rapidly converging phase field model*, Discrete Contin. Dyn. Syst., 15 (2006), pp. 1017–1034.
- [11] G. CAGINALP AND C. ECK, *Rapidly converging phase field models via second order asymptotics*, Discrete Contin. Dyn. Syst., (2005), pp. 142–152.
- [12] G. CAGINALP AND E. A. SOCOLOVSKY, *Efficient computation of a sharp interface by spreading via a phase field method*, Appl. Math. Lett., 2 (1989), p. 117.
- [13] G. CAGINALP AND E. A. SOCOLOVSKY, *Computation of sharp phase boundaries by spreading: The planar and spherically symmetric cases*, J. Comput. Phys., 95 (1991), pp. 85–100.
- [14] X. CHEN, *Spectrums of the Allen–Cahn, Cahn–Hilliard, and phase field equations for generic interfaces*, Comm. Partial Differential Equations, 19 (1994), pp. 1371–1395.
- [15] X. CHEN AND F. REITICH, *Local existence and uniqueness of solutions of the Stefan problem with surface tension and kinetic undercooling*, J. Math. Anal. Appl., 164 (1992), pp. 350–362.
- [16] H. GARCKE AND B. STINNER, *Second order phase field asymptotics for multi-component systems*, Interfaces Free Bound., 8 (2006), pp. 131–157.
- [17] J. W. GIBBS, *Collected Works*, Yale University Press, New Haven, CT, 1948.
- [18] M. E. GLICKSMAN, R. J. SCHAEFER, AND J. D. AYERS, *Dendritic growth—A test of theory*, Met. Trans. A, 7A (1976), pp. 1747–1759.
- [19] S. I. HARIHARAN AND G. W. YOUNG, *Comparison of asymptotic solutions of a phase-field model to a sharp-interface model*, SIAM J. Appl. Math., 62 (2001), pp. 244–263.
- [20] A. KARMA AND W.-J. RAPPEL, *Quantitative phase-field modeling of dendritic growth in two and three dimensions*, Phys. Rev. E (3), 57 (1998), pp. 4323–4349.
- [21] Y. KIM, N. PROVATAS, N. GOLDENFELD, AND J. DANTZIG, *Universal dynamics of phase field models for dendritic growth*, Phys. Rev. E (3), 59 (1999), pp. 2546–2549.
- [22] R. KOBAYASHI, *Modelling and numerical simulation of dendritic crystal growth*, Phys. D, 63 (1993), pp. 410–423.
- [23] R. KOBAYASHI, J. A. WARREN, AND W. C. CARTER, *Vector valued phase field model for crystallization and grain boundary formation*, Phys. D, 119 (1998), pp. 415–423.
- [24] M. B. KOSS, J. C. LACOMBE, L. A. TENNENHOUSE, M. E. GLICKSMAN, AND E. A. WINSA, *Dendritic growth tip velocities and radii of curvature in microgravity*, Met. Mat. Trans. A, 30A (1999), pp. 3177–3190.
- [25] G. LAMÉ AND B. P. CLAPEYRON, *Memoire sur la solidification par refroidissement d’un globe solide*, Ann. Chem. Phys., 47 (1831), pp. 250–256.
- [26] A. M. MEIRMANOV, *On a classical solution of the multidimensional Stefan problem for quasi-linear parabolic equations*, Mat. Sb., 112 (1980), pp. 170–192.
- [27] W. MENDENHALL, *Introduction to Probability and Statistics*, PWS Publishers, Boston, MA, 1987.
- [28] W. MULLINS AND R. F. SEKERKA, *Stability of planar interface during solidification of a dilute binary alloy*, J. Appl. Phys., 35 (1964), pp. 444–451.
- [29] R. H. NOCHETTO AND C. VERDI, *Convergence past singularities for a fully discrete approximation of curvature-driven interfaces*, SIAM J. Numer. Anal., 34 (1997), pp. 490–512.
- [30] J. OCKENDON, *Linear and nonlinear stability of a class of moving boundary problems*, in Free Boundary Problems (Pavia, 1979), E. Magenes, ed., Ist. Naz. Alta Mat. Francesco Severi, Rome, 1980, pp. 443–447.
- [31] L. I. RUBINSTEIN, *The Stefan Problem*, Transl. Math. Monogr. 27, AMS, Providence, RI, 1971.
- [32] R. F. SEKERKA, P. W. VORHEES, S. R. CORIELL, AND G. B. MCFADDEN, *Initial conditions implied by $t^{1/2}$ solidification of a sphere with capillarity and interfacial kinetics*, J. Crystal Growth, 87 (1988), pp. 415–420.
- [33] H. M. SONER, *Convergence of the phase-field equations to the Mullins-Sekerka problem with kinetic undercooling*, Arch. Rational Mech. Anal., 131 (1995), pp. 139–197.
- [34] J. STEFAN, *Über einige Probleme der Theorie der Wärmeleitung*, S.-B. Wien Akad. Mat. Natur., 98 (1889), pp. 473–484.
- [35] S.-L. WANG, R. F. SEKERKA, A. A. WHEELER, B. T. MURRAY, S. R. CORIELL, R. J. BRAUN, AND G. B. MCFADDEN, *Thermodynamically consistent phase-field models for solidification*, Phys. D, 69 (1993), pp. 189–200.